

Published in final edited form as:

J Phys Chem B. 2017 January 12; 121(1): 110–117. doi:10.1021/acs.jpcb.6b11041.

# Ultraslow Domain Motions in HIV-1 TAR RNA Revealed by Solid-State Deuterium NMR

Wei Huang<sup>†</sup>, Prashant S. Emani, Gabriele Varani, Gary P. Drobny<sup>\*</sup>
Department of Chemistry, University of Washington, Box 351700, Seattle, USA 98195

# **Abstract**

Intrinsic motions allow HIV-1 TAR RNA to change its conformation to form a functional complex with the Tat protein, which is essential for viral replication. Understanding of the dynamic properties of TAR necessitates determining motion on the intermediate ns- $\mu$ s time scale. To this end, we performed solid-state deuterium NMR line shape and  $T_{1Z}$  relaxation time experiments to measure intermediate motions for two uridine residues, U40 and U42, within the lower helix of TAR. We infer global motions at rates of  $\sim 10^5 \, \mathrm{s^{-1}}$  in the lower helix, which are much slower than those of the upper helix, indicating the two helical domains reorient independently of one another in the solid-state sample. These results contribute to the aim of fully describing the properties of functional motions in TAR RNA.

#### BRIEFS.

If you are submitting your paper to a journal that requires a brief, provide a one-sentence synopsis for inclusion in the Table of Contents.

### SYNOPSIS.

If you are submitting your paper to a journal that requires a synopsis, see the journal's Instructions for Authors for details.

#### Keywords

HIV-1 TAR RNA; Solid-State NMR; Deuterium; Dynamics

# INTRODUCTION

Many RNAs rely on adaptive conformational changes in response to the binding of small molecules or proteins to fulfill their biological functions. <sup>1–8</sup> The 29-nucleotide HIV-1 transactivation response (TAR) RNA construct provides a paradigmatic example for this class of adaptive RNA recognition events. The UCU bulge and neighboring base pairs in TAR (Figure 1A) are important for the specific binding of viral regulatory protein Tat and

<sup>\*</sup>Corresponding Author: Gary P. Drobny, drobny@chem.washington.edu.
†Present Addresses: Intel Corp, 6505 W Chandler Blvd, Chandler, AZ 85226.
Author Contributions

The manuscript was written through contributions of all authors. All authors have given approval to the final version of the manuscript.

undergo a substantial conformational transition upon protein binding. <sup>1,3,8–13</sup> The structures of TAR in the presence and absence of Tat-derived peptides and argininamide have been widely studied, <sup>1,9,10,14–17</sup> but the dynamic properties of TAR that are the basis of this inherent flexibility still remain of interest. <sup>18–28</sup> The complex superposition of different motional modes that occur with multiple amplitudes and time scales, even for the simple helix–bulge–helix motif of TAR RNA, motivated us to study the 29- nucleotide construct using solid-state NMR. Having previously constructed models for uridine residues in the upper helix and bulge regions, <sup>19</sup> we examine the dynamic behavior of the lower helix in the following work.

Deuterium solid-state NMR line-shape and relaxation experiments, when combined, are sensitive to motions at time scales ranging from nanoseconds to milliseconds. Previous experiments on TAR have shown that it is likely to exhibit motions in this intermediate range of time scales, <sup>22,29</sup> making solid-state NMR an important means of understanding dynamics in TAR RNA. Whereas solution NMR experiments such as relaxation dispersion and the measurement of residual dipolar couplings (RDCs) (see, e.g., Al-Hashimi<sup>7</sup>) can probe the amplitude and degrees of freedom involved, solid-state measurements are uniquely poised to provide a quantitative view of the rates of exchange. This is due to the averaging of interactions on the time scale of the overall diffusive tumbling of the molecule (~a few nanoseconds for TAR RNA<sup>23,30</sup>) in the solution state. Solid-state NMR naturally avoids this rotational averaging. However, it is to be noted that an elegant alternative approach in the solution state was also demonstrated by Al-Hashimi and co-workers: solution NMR <sup>15</sup>N relaxation experiments on TAR constructs, where each domain was elongated separately to slow down overall tumbling, revealed interhelical reorientation motions on a nanosecond time scale.<sup>29</sup> Whereas these results undoubtedly bypass the averaging due to overall rotational tumbling, employing 2H NMR lineshape experiments will further extend the window of sensitivity to the conformational exchange rates to the range from nanoseconds to milliseconds. Site-specific <sup>2</sup>H solid-state NMR studies of TAR RNA were performed by our research group. 18,19 The intermediate rate atomic trajectories of single-stranded U23 and U25 residues at the bulge and U38 within a base pair in the upper helix were fully described. In the current work, 5.6-<sup>2</sup>H deuterium labels were introduced at the U40 and U42 positions in TAR (Figure 1), corresponding to the lower helix and including a member of an unstable base pair that closes the bulge region (U40-A22). RNA samples were hydrated to reproduce conditions in which motions are solution like, using previously established methods of analysis.31

All measurements were performed at room temperature, as was done for previous experiments on the upper helix. Under solid-state conditions, all motions discussed in both the current and previous studies<sup>19</sup> are relative to a fixed, external crystal director frame. Given these conditions, we found that, somewhat surprisingly, deuterium solid-state NMR reveals much slower global motions (twist and bend; see Figure 1A) in the lower helix compared to those in the upper helix. Here, we consider this result and its implications.

# **METHODS**

#### Sample Preparation.

The [5,6-<sup>2</sup>H]-labeled uridine nucleotide was purchased from Thermo Scientific. The deuterated nucleotide was converted to a phosphoramidite, incorporated into the RNA oligonucelotide, and desalted by the manufacturer. No further purification was performed. The sample was checked for homogeneity by analytical denaturing polyacrylamide gel electrophoresis. The following TAR RNA 29-mer constructs were used:

5'-GGCAGAUCUGAGCCUGGGAGCUC\*UCUGCC-3' (U40) and 5'GGCAGAUCUGAGCCUGGGAGCUCUC\*UGCC-3' (U42). U40 (6.7 µmol/62 mg) was dissolved in buffer (50 mM NaCl, 10 mM sodium cacodylate, pH 5.5), then frozen in liquid nitrogen, and lyophilized. There are 10% NaCl and 4.7% cacodylate by weight in the final composition, upon lyophilization. To remove residual HDO and D2O, samples were redissolved in deuterium-depleted water and then lyophilized three times. Each sample was then re-dissolved a final time in deuterium depleted water, annealed in a 90 °C water bath for 5 min, allowed to cool to room temperature for 30 min, and then frozen using liquid nitrogen. The samples were then lyophilized extensively once again to remove residual water. The dry sample was packed into a 5 mm Kel-F rotor. U42 samples (6.7 µmol/62 mg) were prepared using the same procedure. Samples were hydrated by vapor diffusion in a sealed chamber over saturated salt solutions containing deuterium depleted water.<sup>32</sup> Water addition to the samples was monitored gravimetrically. U40 and U42 were hydrated to hydration levels of 8, 16, and 20 water molecules per nucleotide (denoted w = 8, 16, and 20, respectively), with the final mass of water at 28, 56, and 70 mg, respectively. At each hydration level, samples were sealed and allowed to equilibrate an additional week before performing the NMR experiment.

# Solid-State NMR Experiments.

All data collection was performed on a Bruker AVANCE III 500 instrument at 11.74 T field operating at Larmor frequencies of 76.67 MHz for 2H, using a home-built single-channel static deuterium probe. All measurements were performed at room temperature (25 °C) with a 90° pulse time of 2.6 μs. Dwell time for all experiments was 0.4 μs. Recycle delay for all experiments was 1 s. Deuterium line shapes were obtained using a quadrupole echo pulse sequence, <sup>33</sup> which used eight-step phase cycling, with an echo delay of 40 μs. Typical spectra resulted from the acquisition of 300 000-500 000 scans. Line shapes were minimally processed with 200 Hz line broadening and phase correction only. Spin-lattice relaxation times T<sub>1Z</sub> were determined using an inversion recovery pulse sequence, which incorporated a 180° composite pulse to ensure broadband excitation.<sup>34</sup> Typical delays were 1, 10, 25, 50, 100, 500, 1000, and 2000 ms. The quadrupolar-order relaxation times, T1Q, were measured using the broadband Jeener-Broekaert pulse sequence<sup>35,36</sup> with an eight-step phase cycle (similar to that in Olsen et al. <sup>19</sup>). The pulse sequence along with the time delays was as follows:  $90-\tau 1-67-\tau_1-45-\tau_2-45$  [variable relaxation delay]-45-echo delay-90-echo delay-acquisition. Typical delays were  $5\mu s$  for  $\tau 1$ ,  $2.5 \mu s$  for  $\tau 2$ , and 1, 100, 500, 1000, and 2000 ms for the variable relaxation delay, with 40 µs echo delays

# **Data Processing and Motional Models.**

Data processing was performed using Bruker's Topspin 3.0 software. Deuterium line shapes were simulated by the program MXET1<sup>37</sup> using a previously published double two-site jump model of U38, summarized below. 19 Powder-averaged relaxation times T<sub>1Z</sub> were analyzed using a nonlinear least-squares fit of integrated powder spectra to a single exponential. The model for each base was considered to consist of a double two-site jump motion: one motion consisted of a twosite jump rotation of the base (or "base libration") around the base-plane normal, both sites being equally populated; the second involves the simultaneous twisting and bending motion of the entire helical stem containing the labeled residue, relative to a fixed, external crystal director frame (in solid-state conditions, all bulk motions are referenced to a local director coordinate system). The free parameters for the twisting and bending helical motion include a single rate of exchange between two equally populated conformers, as well as one amplitude each for the twist and the bend. These parameters are fit using the deuterium line-shape data because of the sensitivity of the line shape in the rate regime relevant to the helical motion. The faster base-libration model has a jump rate and an angular amplitude that are fit to the relaxation data. The angular amplitude is expressed throughout the article as the half-angle of the full angular excursion of the base; that is, the best-fit amplitude is expressed as  $\pm \theta_{fit}$  °.

The expressions used for the relaxation-time calculations are

$$\frac{1}{T_{1Z}} = \frac{\omega_Q^2}{3} (J_1(\omega_0) + 4J_2(2\omega_0)) \quad (1)$$

$$\frac{1}{T_{1Q}} = \omega_Q^2 J_1(\omega_0) \quad (2)$$

where  $\omega_Q = \frac{3}{4} \frac{e^2 qQ}{\hbar} = 2\pi \left(\frac{3}{4} \frac{e^2 qQ}{\hbar}\right) = 2\pi \left(\frac{3}{4} \nu_{QCC}\right)$  ( $\nu_{QCC}$  is the quadrupolar coupling constant (QCC)) and  $J_m(\omega)$  is the spectral density of order m with the definition

$$J_m(\omega) = 2 \int_0^\infty dt C_m(t) \cos \omega t \quad (3)$$

The powder average correlation function is calculated a

$$\begin{split} \overline{C}_{m}(t) &= \frac{1}{5} \sum_{a=-2}^{2} \left\langle \left( D_{0,a}^{(2)*} \left( \Omega_{PAS \to C}(0) \right) - \left\langle D_{0,a}^{(2)*} \left( \Omega_{PAS \to C}(0) \right) \right\rangle \right) \\ \left( D_{0,a}^{(2)} \left( \Omega_{PAS \to C}(t) \right) - \left\langle D_{0,a}^{(2)} \left( \Omega_{PAS \to C}(t) \right) \right\rangle \right) \right\rangle \end{split} \tag{4}$$

where  $\Omega_{PAS \to C} = (a_{PAS \to C}, \beta_{PAS \to C}, \gamma_{PAS \to C})$  is the set of Euler angles transforming the principal axis system (PAS) of the quadrupole coupling tensor to the crystal director (C)

frame; 
$$D_{m,n}^{(2)}(\Omega_{PAS \to C}) = e^{-im\alpha_{PAS} \to C} d_{mn}(\beta_{PAS \to C}) e^{-in\gamma_{PAS} \to C}$$
 is the second order

Wigner-D rotation matrix for the passive transformation from PAS to C frames. The transformation from the PAS to C frames is broken down into two successive transformations from PAS to a helix-attached, base-perpendicular intermediate (I) frame and from the I frame to the C frame, to deal with two independent motions. Specifically, the Euler angles for each pair of two sites are  $\Omega_{PAS \to C} = \left\{0, \frac{\pi}{2}, \pm \gamma_{libration}\right\}$  and  $\Omega_{I \to C} = \left\{0, 0, \frac{\pi}{2}, \pm \gamma_{libration}\right\}$ 

$$0\} \leftrightarrow \{0, \beta_{bend}, \gamma_{twist}\}.$$

The PAS is defined as being axially symmetric about the C-2H bond with the QCC=179 kHz<sup>38</sup> and asymmetry parameter  $\eta$ =0.<sup>39</sup> In the  $\chi^2$  analysis for the base librations, the parameters for bending and twisting motions were fixed at  $\beta_{bend}$ = 14° and  $\gamma_{twist}$ = -23° and the rate of conformational exchange at 1.2×10<sup>5</sup> s<sup>-1</sup>.

# **RESULTS AND DISCUSSION**

# Effects of Hydration.

In the process of hydrating nucleic acid samples, water is introduced initially to the phosphate backbone, followed by the bases and furanose rings.  $^{40}$  After the completion of local hydration, water populates the bulk hydration layers surrounding the RNA, resulting in a condition that approximates the solution state, as far as we can judge on the basis of the deuterium data in the current and previous studies.  $^{31}$  The dynamics of the upper helix and the bulged loop of TAR RNA have been studied as a function of hydration level, revealing that, at 16-20 water molecules per nucleotide (w =16-20), the effect of hydration on  $T_{1Z}$  and  $T_{1Q}$  of local motions appears to level out. This in turn indicates the local hydration of the nucleic acid backbone and bases is substantially complete.  $^{31}$  The line shape of U38 in the upper helix shows a pronounced drop of amplitude in the center of the Pake doublet line shape from w = 6 to 16 and, thereafter, maintains the same amplitude from hydration levels of w = 16 to 30 (Figure 4 of Olsen et al.  $^{31}$ ), again indicating that hydration of the upper helix is essentially complete by w = 16.

Because of the structural differences between the upper and lower helices, the amount of water required to complete the local hydration of U40 and U42 needs to be established separately as a prerequisite for directly comparing the dynamics observed in the current experiments to that in the previously published work. The  $T_{1Z}$  of both U40 and U42 is around 300 ms at w=8. line shapes for w=8 and 16 (top) and for w=16 and 20 (bottom)

for U40 and U42. The data in Figure 2 show that the line shapes for U40 and U42 do not change markedly between w=16 and 20, indicating that hydration is substantially complete at w=16 for the lower helix. Thus, the line-shape data for U40 and U42 matches the trend observed for U38.  $^{19}$ 

#### Dynamic Models.

The 2H solid-state NMR line shapes of 5,6-2H-labeled U40 and U42 are presented in Figure 3 and compared with that of U38, with all line shapes obtained at sample hydrations of w = 16, where the hydration is inferred to be complete. The line shapes of U40 and U42 are very similar to each other, indicating the existence of similar motions at both sites on the lower helix within the nanaosecond-tomicrosecond intermediate time scale regime. The shapes of the horns of U40/U42 and U38 show similar features as well, but there is a significant difference in the line shapes between the upper and lower helices: a decrease in the intensity at the center of the spectrum for U40 and U42 compared to that of U38. Loss of intensity in the center of a <sup>2</sup>H quadrupolar echo spectrum is caused by motions with correlation times on the order of the echo pulse spacing, which is about 30 µs. 41 In previous studies of base motions in double-stranded DNA,38 slower motions (10-100 µs) observed at higher hydration levels were attributed to the slow, uniform twisting of the entire helix. These slow motions were similarly manifested as a loss of intensity in the center of the 2H quadrupolar echo spectrum, as we see now for U40 and U42. Therefore, the central amplitude reduction features in the line shapes of U40 and U42 reported in Figure 3 are inferred to result from motions on this timescale.

By a quantitative fit to the solid-state data, U38 was found to undergo a combination of  $13^{\circ}$  helical twisting (i.e., a change in the helical twist of  $13^{\circ}$ ) and  $13^{\circ}$  bending (i.e., a change in the helical bend of  $13^{\circ}$ ) motions at a rate of about  $1.4 \times 10^6$  s<sup>-1</sup> corresponding to the global movements of the entire helix, in addition to much faster local base-libration motions ( $\pm 4^{\circ}$ ) at a rate of  $2.2 \times 10^8$  s<sup>-1</sup>. <sup>19</sup> On the basis of this double two-site jump model generated for U38, with local base librations and overall helical bending and twisting, preliminary simulations were performed using the program MXET1<sup>37</sup> for U40 and U42 as well. The local base librations for both U40 and U42 most likely occur at much faster time scales (> $10^8$  s<sup>-1</sup>) and with smaller amplitude relative to the helical motions, as demonstrated for U38. Such motions barely have any visible effect on the line shape, which mostly reports on slower motions. However, as these motions have significant influence on the relaxation times, we extracted the base-libration parameters from fits to  $T_{1Z}$  and  $T_{1Q}$  data at a hydration of w = 16. The measured  $T_{1Z}$  is 146 ms for U40 and 145 ms for U42. The measured  $T_{1Q}$  is 97 ms for U40 and 89 ms for U42. The results of fitting the rate and amplitude parameters (using the Mathematica code) are presented in Figure 4.

The best-fit base-libration amplitudes were in the range of  $\pm 5 - \pm 12^{\circ}$ , with rates on the order of  $4 \times 10^{7} - 2 \times 10^{8} \text{ s}^{-1}$ . Closer examination further restricted the ranges to be  $\pm 10 - \pm 11^{\circ}$  for the amplitude with rates on the order of  $4 \times 10^{7} - 5 \times 10^{7} \text{ s}^{-1}$  for U40 and  $\pm 7 - \pm 11^{\circ}$  for the amplitude with rates on the order of  $4 \times 10^{7} - 1 \times 10^{8} \text{ s}^{-1}$  for U42. However, for the sake of the line-shape simulations presented in Figure 5, we used the best-fit parameters used for the

U38 simulations. The impact of this choice (vs the best-fit values mentioned above) on the line shapes is minimal.

As a precursor to a discussion of the line-shape fitting, it is worth considering the motivation for choosing a helical motion model to explain the line shapes of both U40 and U42. U40 has almost the same 2H line shape as that of U42, and, interestingly, the solid-state deuterium and solution-state 13C relaxation times<sup>22</sup> are also similar for both residues. This is surprising as U40 is near the bulge and many other studies have indicated that the A22-U40 base pair is not stably formed in the absence of Tat protein.<sup>2,23,25</sup> This seems to indicate that the line shape and relaxation times are not sensitive to the motions of U40 that differentiate it from U42. In the absence of such information in our data, we have chosen to model the motion of both residues by a common model of helical reorientation, rather than by two separate models incorporating local dynamic variations. In Figure 5A, we fit the U40 and U42 line shapes changing only the rates of helical domain motions (twisting and bending). A clear trend is observed for the center amplitude, the slower motions causing a greater loss of intensity in the center of the spectrum. A  $\chi 2$  analysis (Figure 5B) was performed for the simulation of the line shape of U42 covering a wide range of rates  $(10^4-10^{10} \,\mathrm{s}^{-1})$ , considering both the motions of the entire helix ("helical rate") and local base librations ("libration rate"). Rates of twisting and bending of the entire lower helix on the order of  $10^5$  s<sup>-1</sup> describe the data well; these rates are ~10 times slower than the corresponding motions for the upper helix of TAR but comparable to the motional rates observed in double-stranded DNA.<sup>38</sup> Figure 5C presents the line shapes corresponding to helical motions with differing amplitudes at a rate of  $1.4 \times 10^5 \, \mathrm{s}^{-1}$  obtained from simulations, showing the significant change in the horns that occur with large-amplitude motion. No such change in the horns is observed for U40 and U42, indicating that only smallamplitude motions occur. A  $\chi^2$  analysis (Figure 5D) was also performed for the simulation of the line shape of U42, covering the 0-50° range of helical domain motions. The best-fit amplitudes for the helical motion include a 0-18° bend and a 18-25° twist, with a  $\chi$ 2 under 1.5.

#### **Differences in Helical Motion Time Scales.**

Given that the motion of the upper helix reported in Olsen et al. 2010<sup>19</sup> occurs at rates faster than those observed for the lower helix, it is important to consider the influence of the solid-state intermolecular interactions on the dynamics: (a) For particular hydration states and ionic concentrations in the environment of the molecule, what are the types and magnitudes of the forces that restrict the tumbling of the molecule? (b) Do these restrictive forces affect the different domains of the molecule differently? The discussion on solid-state conditions can, in fact, be seen as an extension of the same considerations as those used for RDCs (e.g., the discussions involved in the simulation of both steric<sup>42</sup> and electrostatic<sup>43</sup> alignments). On account of the charged phophodiester backbones, the alignment of RNA molecules due to neighboring molecules is likely to be a combination of steric and electrostatic effects, dependent on the water and buffer concentrations in the interstices. The effects may also be nonuniform. One could imagine the extreme case, where one of the helices experiences a very restrictive, deep intermolecular potential, whereas the other moves within a shallow, broad free-energy surface. In this case, the more restricted domain will move at a faster rate

(the largest few rate eigenvalues of the motion for a potential with more rapid variation will be larger) and with a smaller amplitude than the other domain. Of course, as simulations consider averages over the entire sample, this would demand a uniformly different restriction potential for the two domains across all molecules in the sample. This may arise as a result of a slight difference in hydration (though similar results were obtained from the NMR data discussed here), differences in ionic concentrations, or the impact of the hairpin loop attached to the upper helix. The essential point is that an a priori prediction of the collective motions of the two helical domains is not possible without a consideration of the sample conditions and the consequent variations in constraints on domain motion. Thus, the interpretation of solid-state NMR data is carried out in terms of motions relative to an external crystal director frame, and descriptions of interdomain motions are potentially obfuscated. It is also worth reiterating the point that solid-state and solution motions are not expected to be identical in the most general case. The effect of water on the entire molecule or on its parts is significant and may impact rates, amplitudes, and even the participating degrees of freedom in the motion of the molecule. The more likely motions to cross over faithfully from one set of sample conditions to another are those with smaller amplitudes and with a smaller foray into the intermolecular interstices. Larger domain motions may be impacted by the concentration of the sample and thus vary from solid state to solution. Of course, this must also be consistent with the conclusions made in the preceding sections regarding the change in motions as a function of the change in hydration in the solid state: our understanding is that although the solid state line shapes do converge above a certain hydration level, clearly this hydration level is not sufficient to cause full tumbling of the molecule, thus representing an intermediate motional "plateau" in the continuum between solid-state and solution conditions.

#### Study of Interhelical Motions.

Given the absence of detailed simulations of the solid-state sample environment, we instead previously carried out a model-based approach, where the solid-state-inspired models were incorporated into a tumbling molecule and fit to solution <sup>13</sup>C relaxation times.<sup>23,24</sup> This enabled us to check the consistency of the solid-state models in a solution context. We found that the solution relaxation times can be fit by local motions on a similar time scale and interhelical motions on a slower time scale than those observed in solid-state conditions, with the aforementioned caveat that solid-state helical models are assessed relative to an external frame, whereas solution models involve interhelical motions. We discuss the results here to provide a larger context for the solid-state models of the current work. The goal of these papers<sup>23,24</sup> was to introduce models motivated by solid-state results into a molecule that is both tumbling in solution and changing its conformation through discrete jumps. This was enabled by a theoretical and numerical framework that calculated solution relaxation times by solving the rotational diffusion equation<sup>24</sup> and using an RDC-selected subensemble of conformations generated by the Rosetta program FARFAR<sup>44</sup> to build a dynamic trajectory.23 The methodology also interestingly extends the sensitivity of the <sup>13</sup>C relaxation rates to time scales slower than the expected ñanosecond scale, as the potentially slower process of conformational exchange impacts the diffusion tensors that are sampled during the course of rotational tumbling, which occurs on the ñanosecond scale. Thus, there is a reflection of the slower exchange process in the nanosecond-sensitive <sup>13</sup>C relaxation times,

making the results derived therefrom relevant to the discussion here. The base-libration parameters from early experiments presented in this work, in combination with those from the U38 study, <sup>19</sup> were used as a starting point in a solution-state NMR analysis of helical residues.<sup>23</sup> Initializing the baselibration parameter search with the values from the solidstate studies led to a best-fit rate for the solution-state relaxation times in the range of  $10^{7}$ – $10^{9}$  s<sup>-1</sup> and amplitudes less than  $\sim \pm 20^{\circ}$  when all of the helical residues in the entire sample were considered. Thus, the range of libration parameters in the solution state did not stray away from the solid-state values presented in this article during the course of parametric search procedure. Interestingly, the best fit for the solution state was obtained when all of the upper helical residues and U40 and U42 on the one hand and all of the remaining lower helix residues on the other hand were simulated with two separate groups of local base parameters. The best-fit solution interhelical exchange rates (as combined twisting and bending rates) are in general slower than the rate of  $1.4 \times 10^6$  s<sup>-1</sup> reported for U38 in the upper helix<sup>19</sup> and those for U40 and U42 reported here, occurring in the range of 10<sup>4</sup>– 10<sup>5</sup> s<sup>-1</sup>. The best-fit amplitudes are understandably larger in solution conditions, with exchanges between conformational states separated by up to ~90° interhelical bends and ~140° interhelical twists. There are pairs of conformers (among the set of highly populated states) in which the changes in the bend angles are similar to those observed for the lower helix in this work, but given the aforementioned difficulty in describing interhelical dynamics in solid-state analyses, this may not be more than a numerical coincidence. In summary, the base-libration parameters from solution simulations are similar to those observed in the solid state, whereas the helical amplitudes were larger and the helical rates were smaller (i.e., the motions were slower) in the solution state relative to those in the solid-state models.

#### Comparisons to Other Studies.

As with solution conditions, given that the referencing of solid-state motions is done relative to an external crystallite frame, it is difficult to exactly quantify the overall amplitudes of the interhelical motions to which RDC data are sensitive. A simple calculation would add together the maximum excursions of the upper and lower helices relative to the external frame in quadrature to produce maximum interhelical bend changes on the order of 13-25°. Previous solution RDC NMR studies <sup>10,45</sup> show a ~45° bend in the interhelical angle. Thus, the solid-state data indicate a more rigid molecule in the solid state relative to that described by RDC studies, similar to the results for the solution state described in the previous section. As it was reported that motions in TAR are strongly dependent on the ionic strength and have much smaller amplitudes under moderate to high ionic strength conditions<sup>46</sup> and our solid-state samples have much higher ionic strength, the smaller amplitudes observed here could also be due to these differences (in addition to other considerations of restriction in the solid state). To provide a sense of the ionic strength of a solid-state sample, we consider the case of the U40 sample with w = 16. The sample contains 1.99 mg of NaCl and 15.5 mg of H<sub>2</sub>O. We do not usually measure the volume of sample in solid-state NMR and so, instead, if we used the density of water to do an estimation, the ionic strength is

$$\frac{\text{no. of moles of NaCl}}{\text{volume of sample (:volume of water)}}$$

$$= \left(\frac{1.99 \text{ mg NaCl}}{58 \text{ g/mol}}\right) \left(\frac{15.5 \text{ mg H}_2\text{O}}{1 \text{ g/mL}}\right)$$

$$= 22.13 \text{mM}$$

The real volume is larger, but the ionic strength should still be much higher than that of a solution sample. Using a domain-elongation strategy, Al-Hashimi et al.<sup>20</sup> reported that a network of local and collective motions occurring at nanosecond time scales underlies the RNA's ability to adaptively change conformation. Solid-state NMR studies found domain reorientational motions within the upper helix occurring at much longer time scales of 10<sup>6</sup> s  $^{-1}$ , 19 whereas the results of the current article indicate motions on the order of  $10^5$  s<sup>-1</sup> for the lower helix. Further studies by our group matching solution <sup>13</sup>C relaxation times indicated that interhelical motions occurred on a slow time scale on the order of 10<sup>4</sup>–10<sup>5</sup> s <sup>-1</sup>.23,24 The mutual consistency of the three results can be considered as follows: (a) the solid-state 2H studies are sensitive to motions on the nanosecond-to millisecond time scale, but the local environment of a molecule, including both ionic concentrations and steric and electrostatic interactions with neighboring molecules, may differentially impact the two helices, resulting in two different rates of conformational exchange; (b) solution <sup>15</sup>N relaxation-time measurements on elongated TAR are sensitive to motional time scales up to several nanoseconds and may reveal modes of conformational exchange not modeled in the current analysis; (c) solution <sup>13</sup>C relaxation times, usually sensitive to time scales up to several nanoseconds, gain sensitivity to longer conformational exchange time scales due to the fluctuating diffusion tensors and thus probe slower modes of interhelical reorientation. There is no apparent inconsistency between (a) and (c) as the solid-state motions could transition to the slower motions observed using the <sup>13</sup>C relaxation times once the restrictions of the solid-state environment are removed. However, the solid-state data here fits with the simplest possible model that may obscure the presence of nanoscale motions observed in the <sup>15</sup>N data. Thus, it is possible that there are several modes with different time scales superimposed on each other. Future modeling exercises will have to consider this potentially complex superposition of modes.

# **CONCLUSIONS**

The dynamics of two uridine residues, U40 and U42, in the lower helix of HIV-1 TAR RNA was investigated using solid state <sup>2</sup>H NMR line-shape and relaxation-time analyses. We fit the data using models that indicate that the lower helix underwent conformational exchange between two conformers at a rate an order of magnitude slower compared to that obtained using similar models for the upper helix, occurring at rates of about 10<sup>5</sup> s<sup>-1</sup>. The differences observed between the two helices and between the solid-state models in this work and relaxation data from solution analyses can be partially explained by the restriction inherent in a solid-state sample and the high ionic strength, which likely play a significant role in determining the dynamics. Additional considerations include the possible superposition of multiple dynamic modes that necessitate more complicated models.

# ACKNOWLEDGMENT

G.P.D. acknowledges the NIH grant RO1-GM109417.

#### **ABBREVIATIONS**

**HIV** Human Immunodeficiency Virus

**TAR** Trans-Activation Response

NMR Nuclear Magnetic Resonance

# **REFERENCES**

(1). Puglisi JD; Tan R; Calnan BJ; Frankel AD; Williamson JR Conformation of the TA RNA-Arginine Complex by NMR Spectroscopy. Science (80-.). 1992, 257 (5066), 76–80.

- (2). Aboul-ela F; Karn J; Varani G The Structure of the Human Immunodeficiency Virus Type-1 TAR RNA Reveals Principles of RNA Recognition by Tat Protein. J Mol Biol 1995, 253 (2), 313–332. [PubMed: 7563092]
- (3). Leulliot N; Varani G Current Topics in RNA-Protein Recognition: Control of Specificity and Biological Function through Induced Fit and Conformational Capture. Biochemistry 2001, 40 (27), 7947–7956. [PubMed: 11434763]
- (4). Williamson JR Induced Fit in RNA Protein Recognition. 2000, 7 (10), 834–837.
- (5). Al-Hashimi HM Dynamics-Based Amplification of RNA Function and Its Characterization by Using NMR Spectroscopy. ChemBioChem 2005, 6 (9), 1506–1519. [PubMed: 16138302]
- (6). Draper DE Themes in RNA-Protein Recognition. J Mol Biol 1999, 293 (2), 255–270. [PubMed: 10550207]
- (7). Al-Hashimi HM NMR Studies of Nucleic Acid Dynamics. J. Magn. Reson 2013, 237, 191–204. [PubMed: 24149218]
- (8). Borkar AN; Bardaro MF; Camilloni C; Aprile FA; Varani G; Vendruscolo M Structure of a Low-Population BindingIntermediate in Protein-RNA Recognition. Proc. Natl. Acad. Sci. U.S.A 2016, 113, 7171–7176. [PubMed: 27286828]
- (9). Aboul-ela F; Karn J; Varani G; Aboul-ela F The Structure of the Human Immunodeficiency Virus Type-1 TAR RNA Reveals Principles of RNA Recognition by Tat Protein. J. Mol. Biol 1995, 253 (2), 313–332. [PubMed: 7563092]
- (10). Aboul-ela F; Karn J; Varani G Structure of HIV-1 TAR RNA in the Absence of Ligands Reveals a Novel Conformation of the Trinucleotide Bulge. Nucleic Acids Res 1996, 24, 3974–3981. [PubMed: 8918800]
- (11). Long KS; Crothers DM Interaction of HumanImmunodeficiency Virus Type 1 Tat-Derived Peptides with TAR RNA. Biochemistry 1995, 34, 8885–8895. [PubMed: 7612630]
- (12). Pritchard CE; Grasby JA; Hamy F; Zacharek AM; Singh M; Karn J; Gait MJ Methylphosphonate Mapping of Phosphate Contacts Critical for RNA Recognition by the Human Immunodeficiency Virus Tat and Rev Proteins. Nucleic Acids Res 1994, 22, 2592–2600. [PubMed: 8041622]
- (13). Churcher MJ; Lamont C; Hamy F; Dingwall C; Green SM; Lowe AD; Butler PJG; Gait MJ; Karn J High Affinity Binding of TAR RNA by the Human Immunodeficiency Virus Type-1Tat Protein Requires Base-Pairs in the RNA Stem and Amino Acid Residues Flanking the Basic Region. J. Mol. Biol 1993, 230, 90–110. [PubMed: 8450553]
- (14). Calnan BJ; Tidor B; Biancalana S; Hudson D; Frankel AD Arginine-Mediated RNA Recognition: The Arginine Fork. Science 1991, 252 (5009), 1167–1171. [PubMed: 1709522]
- (15). Davidson A; Leeper TC; Athanassiou Z; Patora-Komisarska K; Karn J; Robinson JA; Varani G Simultaneous Recognition of HIV-1 TAR RNA Bulge and Loop Sequences by Cyclic Peptide Mimics of Tat Protein. Proc. Natl. Acad. Sci. U.S.A 2009, 106, 11931–11936. [PubMed: 19584251]

(16). Huang W; Varani G; Drobny, G. P. C / 15 N - 19 F Intermolecular REDOR NMR Study of the Interaction of TAR RNA with Tat Peptides. 2010, 23, 17643–17645.

- (17). Huang W; Varani G; Drobny GP Interactions of Protein Side Chains with RNA Defined with REDOR Solid State NMR. J. Biomol. NMR 2011, 51 (3), 347–356. [PubMed: 21947838]
- (18). Olsen GL; Echodu DC; Shajani Z; Bardaro MF; Varani G; Drobny GP Solid-State Deuterium NMR Studies Reveal Micros-Ns Motions in the HIV-1 Transactivation Response RNA Recognition Site. J. Am. Chem. Soc 2008, 130 (10), 2896–2897. [PubMed: 18275190]
- (19). Olsen GL; Bardaro MF; Echodu DC; Drobny GP; Varani G Intermediate Rate Atomic Trajectories of RNA by Solid-State NMR Spectroscopy. J. Am. Chem. Soc 2010, 132 (1), 303–308. [PubMed: 19994901]
- (20). Zhang Q; Sun XY; Watt ED; Al-Hashimi HM Resolving the Motional Modes That Code for RNA Adaptation. Science (80-.). 2006, 311 (5761), 653–656.
- (21). Zhang Q; Stelzer AC; Fisher CK; Al-Hashimi HM Visualizing Spatially Correlated Dynamics That Directs RNA Conformational Transitions. Nature 2007, 450 (7173), 1263–U14. [PubMed: 18097416]
- (22). Bardaro MF; Shajani Z; Patora-Komisarska K; Robinson JA; Varani G How Binding of Small Molecule and Peptide Ligands to HIV-1 TAR Alters the RNA Motional Landscape. Nucleic Acids Res 2009, 37 (5), 1529–1540. [PubMed: 19139066]
- (23). Emani PS; Bardaro MF; Huang W; Aragon S; Varani G; Drobny GP Elucidating Molecular Motion through Structural and Dynamic Filters of Energy-Minimized Conformer Ensembles. J. Phys. Chem. B 2014, 118 (7), 1726–1742. [PubMed: 24479561]
- (24). Emani PS; Olsen GL; Varani G; Drobny GP Theory of Nonrigid Rotational Motion Applied to NMR Relaxation in RNA. J. Phys. Chem. A 2011, 115 (44), 12055–12069. [PubMed: 21870804]
- (25). Salmon L; Bascom G; Andricioaei I; Al-Hashimi HM A General Method for Constructing Atomic-Resolution RNA Ensembles Using NMR Residual Dipolar Couplings: The Basis for Interhelical Motions Revealed. J. Am. Chem. Soc 2013, 135, 5457–5466. [PubMed: 23473378]
- (26). Merriman DK; Xue Y; Yang S; Kimsey IJ; Shakya A; Clay M; Al-Hashimi HM Shortening the HIV-1 TAR RNA Bulge by a Single Nucleotide Preserves Motional Modes over a Broad Range of Time Scales. Biochemistry 2016, 55, 4445–4456. [PubMed: 27232530]
- (27). Xue Y; Gracia B; Herschlag D; Russell R; Al-Hashimi HM Visualizing the Formation of an RNA Folding Intermediate through a Fast Highly Modular Secondary Structure Switch. Nat. Commun 2016, 7, No. ncomms11768.
- (28). Fonseca R; van den Bedem H; Bernauer J Probing RNA Native Conformational Ensembles with Structural Constraints. J. Comput. Biol 2016, 23, 362–371. [PubMed: 27028235]
- (29). Zhang Q; Stelzer AC; Fisher CK; Al-Hashimi HM Visualizing Spatially Correlated Dynamics That Directs RNA Conformational Transitions. Nature 2007, 450 (7173), 1263–1267. [PubMed: 18097416]
- (30). Emani PS; Olsen GL; Echodu DC; Varani G; Drobny GP Slow Exchange Model of Nonrigid Rotational Motion in RNA for Combined Solid-State and Solution NMR Studies. J. Phys. Chem. B 2010, 114 (48), 15991–16002. [PubMed: 21067190]
- (31). Olsen GL; Bardaro MF; Echodu DC; Drobny GP; Varani G Hydration Dependent Dynamics in RNA. J. Biomol. NMR 2009, 45 (1–2), 133–142. [PubMed: 19669102]
- (32). Weast RC CRC Handbook of Chemistry and Physics, 60th Ed.; CRC Press: Boca Raton, FL, 1979.
- (33). Davis JH Deuterium Magnetic Resonance Study of the Gel and Liquid Crystalline Phases of Dipalmitoyl Phosphatidylcholine. Biophys. J 1979, 27, 339–358. [PubMed: 263690]
- (34). Tycko R Broadband Population Inversion. Phys. Rev. Lett 1983, 51, 775–777.
- (35). Wimperis S; Bodenhausen G Broadband Excitation of Quadrupolar Order by Modified Jeener-Broekaert Sequences. Chem. Phys. Lett 1986, 132, 194–199.
- (36). Hoatson GL Broadband Composite Excitation Sequences for Creating Quadrupolar Order in 2H NMR. J. Magn. Reson 1991, 94, 152–159.
- (37). Greenfield MS; Ronemus AD; Vold RL; Vold RR; Ellis PD; Raidy TE Deuterium Quadrupole-Echo NMR Spectroscopy. III. Practical Aspects of Lineshape Calculations for Multiaxis Rotational Processes. J. Magn. Reson 1987, 72 (1), 89–107.

(38). Kintanar A; Huang WC; Schindele DC; Wemmer DE; Drobny G Dynamics of Bases in Hydrated [d(CGCGAATTCGCG)]2. Biochemistry 1989, 28 (1), 282–293. [PubMed: 2706252]

- (39). Vold RR; Vold RL Deuterium Relaxation in Molecular Solids. In Advances in Magnetic and Optical Resonance; Academic Press, Inc, 1991; Vol. 16, pp 85–171.
- (40). Falk M; Lord RC; Hartman KA HYDRATION OF DEOXYRIBONUCLEIC ACID .1. A GRAVIMETRIC STUDY. J. Am. Chem. Soc 1962, 84 (20), 3843–3846.
- (41). Spiess HW; Sillescu H Solid Echoes in the Slow-Motion Region. J. Magn. Reson 1981, 42 (3), 381–389.
- (42). Zweckstetter M; Bax A Prediction of Sterically Induced Alignment in a Dilute Liquid Crystalline Phase: Aid to Protein Structure Determination by NMR. J. Am. Chem. Soc 2000, 122, 3791–3792
- (43). Zweckstetter M; Hummer G; Bax A Prediction of Charge-Induced Molecular Alignment of Biomolecules Dissolved in Dilute Liquid-Crystalline Phases. Biophys. J 2004, 86, 3444–3460. [PubMed: 15189846]
- (44). Das R; Karanicolas J; Baker D Atomic Accuracy in Predicting and Designing Noncanonical RNA Structure. Nat. Methods 2010, 7, 291–294. [PubMed: 20190761]
- (45). Al-Hashimi HM; Gosser Y; Gorin A; Hu WD; Majumdar A; Patel DJ Concerted Motions in HIV-1 TAR RNA May Allow Access to Bound State Conformations: RNA Dynamics from NMR Residual Dipolar Couplings. J. Mol. Biol 2002, 315 (2), 95–102. [PubMed: 11779230]
- (46). Casiano-Negroni A; Sun XY; Al-Hashimi HM Probing Na+-Induced Changes in the HIV-1 TAR Conformational Dynamics Using NMR Residual Dipolar Couplings: New Insights into the Role of Counterions and Electrostatic Interactions in Adaptive Recognition. Biochemistry 2007, 46 (22), 6525–6535. [PubMed: 17488097]

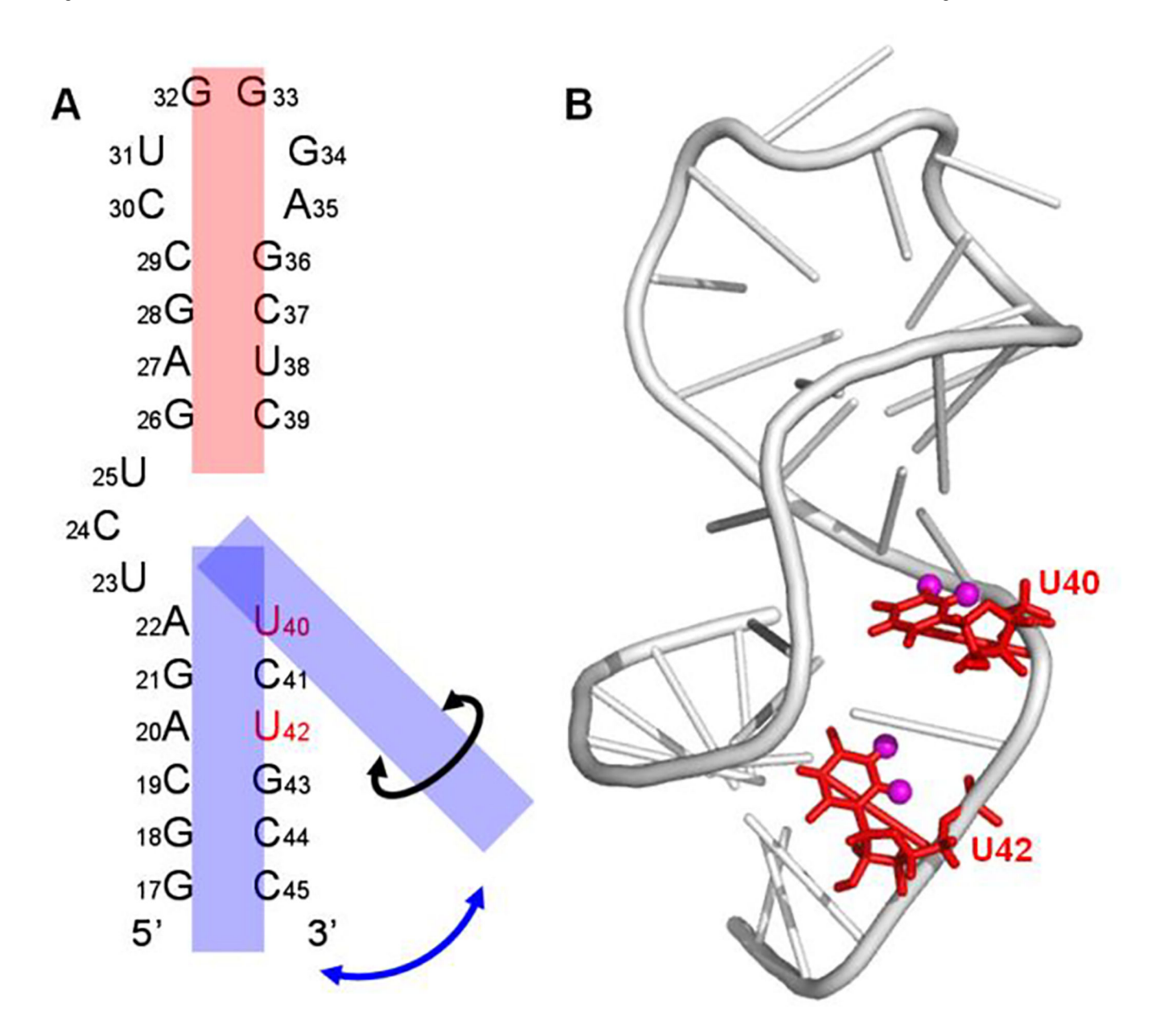


Figure 1.
a) Secondary structure of TAR RNA, indicating the position of the 5,6-<sup>2</sup>H labeled U40 and U42 nucleotides. The upper helical domain is represented by a red rectangle, while the lower helical domain is represented by a blue rectangle instead. The blue arrow represents the bending motion of the lower helix, and the black arrow represents the twist. b) 3D Structure of the unbound TAR RNA.<sup>11</sup> The phosphate backbone is represented by a grey ribbon, with U40 and U42 indicated in red. The labeled <sup>2</sup>H is shown in magenta.

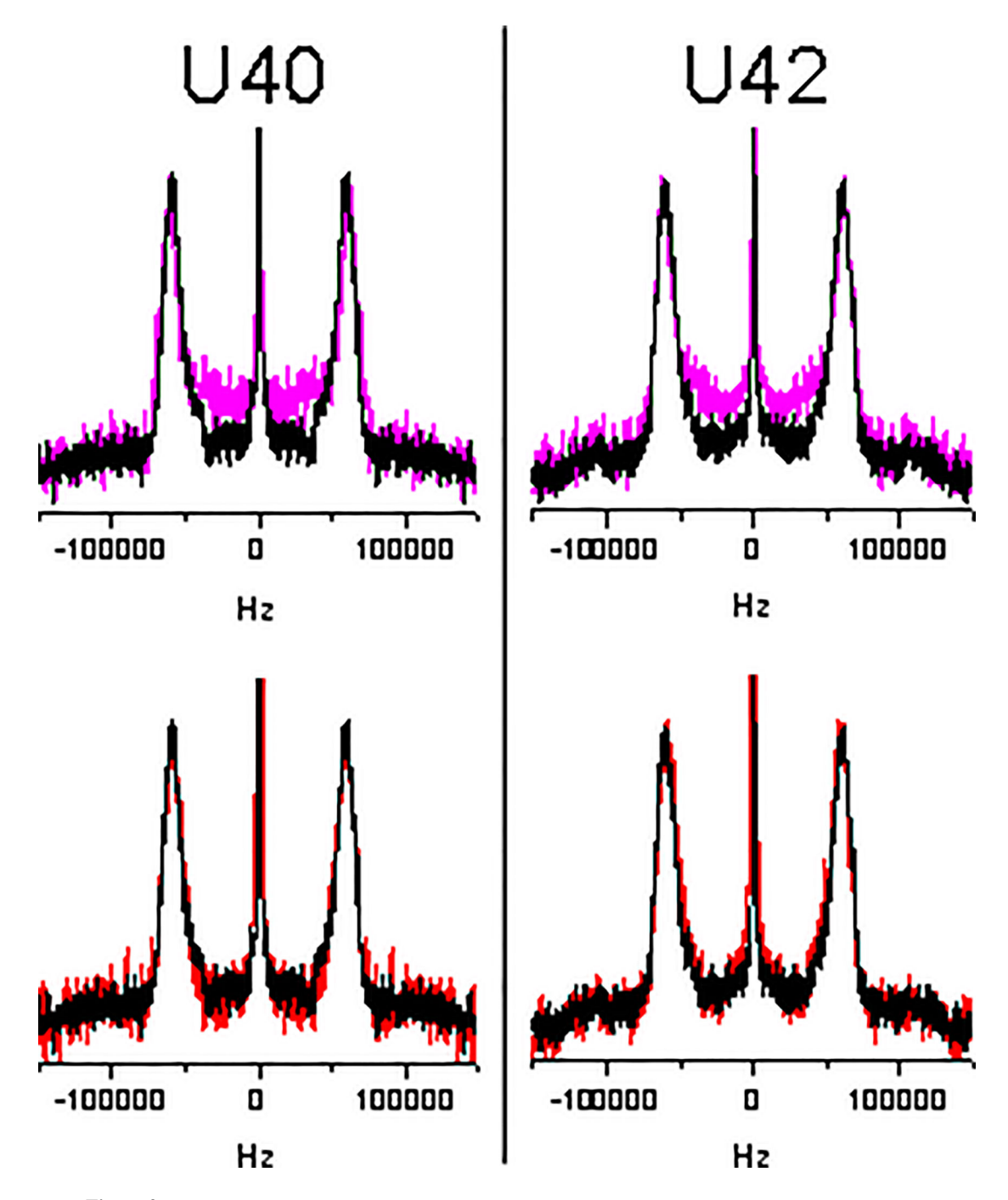


Figure 2. Solid-state  $^2H$  NMR line shapes for U40 and U42 in TAR RNA at different hydration levels. Top: Overlays of the line shapes for w=8 (magenta) and w=16 (black). Bottom: Overlays of the line shapes for w=16 (black) and w=20 (red). The signal in the center of the spectrum is dominated by the sharp peak corresponding to residual  $^2H$  signal in the deuterium-depleted water.

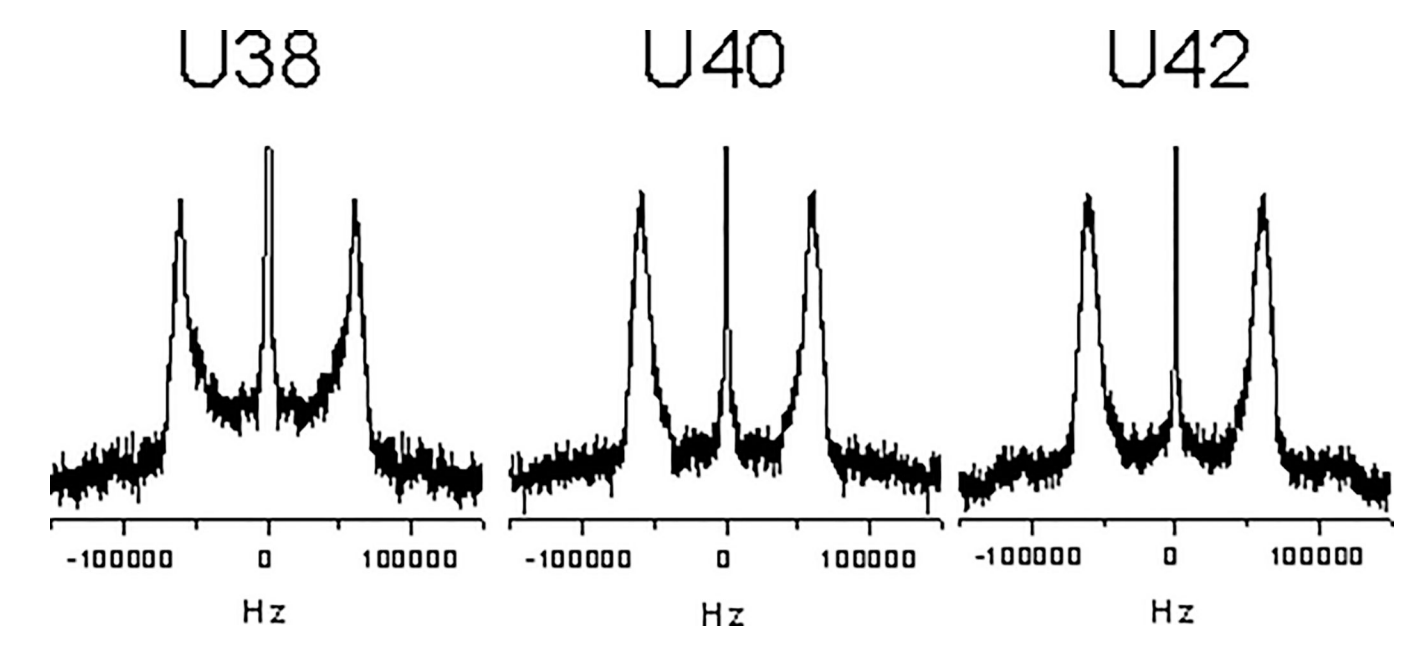


Figure 3. Solid-state  ${}^2H$  NMR line shapes at a hydration of w = 16 for U38,  ${}^{16}$  U40 and U42 in TAR RNA. U40 and U42 are measured under the same experimental conditions as previously reported for U38 in order to make full comparisons.

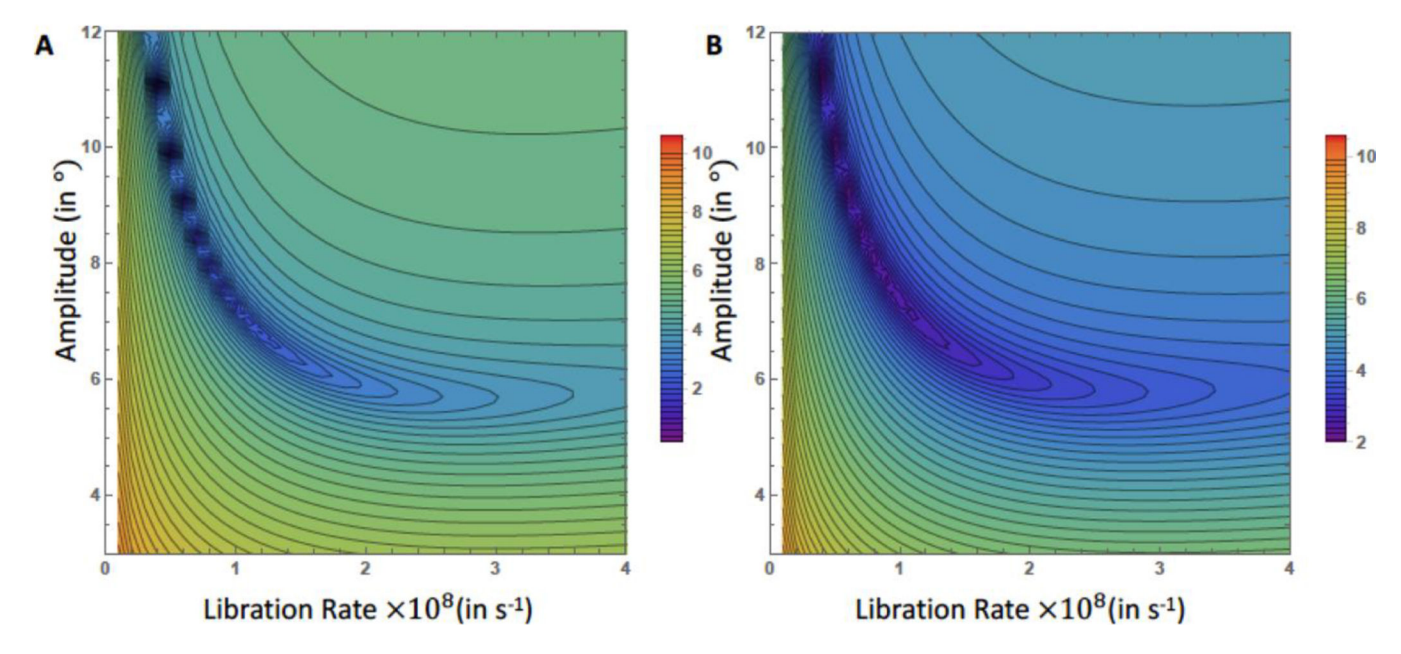


Figure 4. Contour plots for the fits of the rate (in units of ×108 s-1) and amplitude (for a two-site jump expressed as  $\pm \theta$  fit ° relative to the average position in units of degrees) parameters, where the measure of the fit is given as  $\log \left( \sqrt{\left(T_{1Z} - T_{1Z}^{\text{exp}t}\right)^2 - \left(T_{1Q} - T_{1Q}^{\text{exp}t}\right)^2} \right)$  Results are provided for (A) U40 and (B) U42.

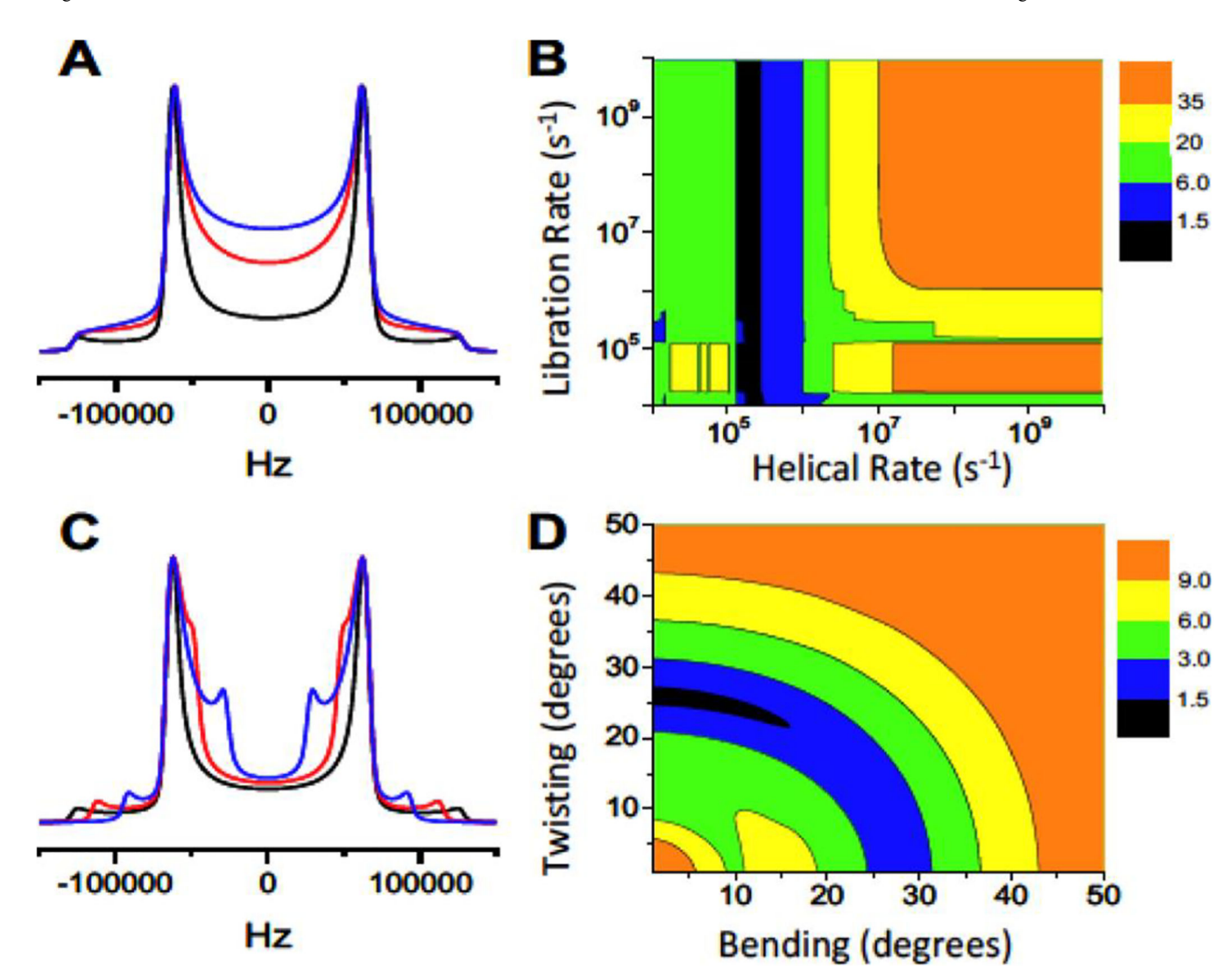


Figure 5. (A) MXET1<sup>28</sup> line shape fits to experimental data for U42 conducted by varying the rate of helical domain motion  $(1.4 \times 10^5 \text{ s}^{-1} \text{ in black}, 1.4 \times 10^6 \text{ s}^{-1} \text{ in red}, 1.4 \times 10^7 \text{ s}^{-1} \text{ in blue})$ . Other parameters of the simulations correspond to the same values published for U38.<sup>16</sup> (B) Contour plot of a  $\chi^2$  analysis indicating the region of best fit for the rate of motions of U42. Rate 1 corresponds to helical domain motions, including twisting and bending; rate 2 refers to the rate of local base librations. (C) MXET1<sup>28</sup> line shape simulation conducted by varying the amplitude of helical domain motion (13° in black, 26° in red, 39° in blue). The rate of helical domain motion is kept at  $1.4 \times 10^5 \text{ s}^{-1}$ . Other parameters of the simulations coincide with those published for U38<sup>16</sup>. (D) Contour plot of a  $\chi^2$  analysis indicating the region of best fit for the amplitude of motions of U42 (twisting and bending).